LRP 418/90 September 1990

Invited and Contributed Papers
presented at the

15th INTERNATIONAL CONFERENCE ON INFRARED AND MILLIMETER WAVES

Lake Buena Vista, Orlando, Florida, U.S.A.
December 10-14, 1990

TABLE OF CONTENT

REVIEW OF GYROTRON DEVELOPMENT AT THE CENTRE DE RECHERCHES EN PHYSIQUE DES PLASMAS

The CRPP/ABB Gyrotron Development Group
presented by M.Q. Tran

Centre de Recherches en Physique des Plasmas
Association Euratom - Confédération Suisse
Ecole Polytechnique Fédérale de Lausanne
21, Av. des Bains, CH-1007 Lausanne, Switzerland

ABSTRACT

Gyrotron development activities at the Centre de Recherches en Physique des plasmas in Lausanne are directed along two directions, quasi optical gyrotrons and, with less emphasis, cylindrical cavity gyrotrons. This paper will review the recent work performed in these two fields.

1. INTRODUCTION

The Centre de Recherches en Physique des Plasmas has been actively involved in the development of both quasi-optical (Q.O.) and cylindrical cavity gyrotrons with an emphasis on the Q.O. concept. Some new theoretical work has been performed, which may provide some clue for the understanding of the problem of the modest efficiency obtained so far in all Q.O. gyrotrons. Recent progress has also been made in the field of output coupling

Using a cylindrical cavity gyrotron operating as a Backward Wave Oscillator, we have tested a novel method to measure the α of the electron beam. A 39GHz TE_{02} gyrotron has also been built and installed on the TCA tokamak of our laboratory.

2. QUASI-OPTICAL GYROTRON

a) Operation at fundamental

The results obtained so far on our Q.O. gyrotron are described in a recent publication [1]. Power up to 90kW with an efficiency close to 12% has been achieved. The optimization was performed while maintaining the magnetic field in the interaction region fixed. At high value of beam current I, the frequency of the oscillations increased (Fig. 1): a variation of about four longitudinal modes (i.e. 1.76GHz) was measured. The interpretation of the observed frequency shift with I should involve the change in the electron beam voltage depression ΔV in the beam tunnel and the interaction region. With our beam parameters, ΔV is of the order of 8kV at 10A. We have computed the non-linear efficiency of the Q.O. gyrotron taking into account the beam depression in the interaction region [2]. The boundary conditions are modelized as a conducting cylinder of a diameter equal to the mirror separation d and length l equal to the distance between the two upstream and downstream beam tunnels (l= 12cm). At the entrance of the interaction region, ΔV is assumed to be null. The multimode calculations [3], including the effect of ΔV along the beam trajectory, indicate that the whole spectrum is shifted by four modes at I above 10A compared to the case where ΔV is

neglected as shown in figure 2.The efficiency is about 14% at 10A, slightly above the value obtained when ΔV is neglected (10.3%).

The results of the previous calculations also point out that means to control the detuning migth be necessary, if the optimum detuning could not be achieved via multimode interaction (Fig. 2). In a pulsed experiment, a variation in time of the beam voltage V_b could change the detuning at a given I, provided that the mode is stable. We have verified by numercal computation that, for example, a change in V_b from 70kV to 80kV can modify drastically the output power and efficiency compared to the case without voltage change.The result of such simulation is presented in figure 3. The voltage V_b is suddenly increased by 10kV at time t=750ns in the simulation, when the system has reached an equilibrium state corresponding to V_b =70kV. The power jumps from 700kW to more than 1.2MW.

b) Oscillations at second harmonic

The gyrotron was designed to operate at the fundamental. Second harmonic emission was also observed simultaneously with the fundamental [4]. Its frequency is exactly twice the one emitted at the fundamental. It also leads to a decrease of the total power.

A multimode code which includes both the fundamental and the second harmonic has been developed [5]. The simulation indicates that the second harmonic affects only weakly the fundamental.

c) Output coupling

To allow an efficient transport and launching of the r.f. wave in the plasma, a gaussian output is desired. We have recently cold tested resonators, one mirror of which is a grating arranged in the Littrow mount. A gaussian output was measured with a high coupling efficiency (larger than 85%) (Fig. 4) [6].

d) Test of a compact Q.O. gyrotron

A compact Q.O. gyrotron deisgned to operate at 92GHz has been built [7]. Results from the tests will be presented.

3. CYLINDRICAL CAVITY GYROTRON

a) Beam diagnostic using the backward wave

In the 8GHz gyrotron, backward wave oscillations (BWO) in the frequency range around 7GHz in the TE_{21} mode have been observed. By measuring the frequency of the BWO and comparing it with the predictions of the nonlinear self-consistent code, it is possible to infer the value of the velocity ratio α. A good agreement was found with the values given by the EGUN particle trajectory code (Fig. 5) [8].

b) 39GHz gyrotron

A TE_{02} gyrotron at 39GHz has been constructed and installed on the TCA tokamak to study the effectiveness of ECRH assisted startup [9]. The choice of the frequency 39GHz was motivated by the value of the toroidal field of the present TCA tokamak and TCV, the tokamak under construction. In the preliminary phase of operation, power level larger than 230kW was obtained at 8A at an efficiency larger than 35%. 98% of the power was found in the desired TE_{02} mode. Tests are still under way to increase the current and power and the results of the optimization will be presented.

ACKNOWLEDGEMENTS

This work was supported in part by the "CERS", the "FNSRS", the "OFEN", by NET and by internal R&D funds from ABB-Infocom SA.

REFERENCES

[1] S. Alberti et al., Phys. Fluids **B2**, 1654, (1990)

[2] S. Alberti et al., submitted to Phys. Fluids **B2**

[3] A. Bondeson et al., Millimeter and Infrared Waves **9**, K. Button ed. (Academic Press) p. 309 (1983)

[4] S. Alberti et al., to be published in Phys. Fluids **B2**, November 1990

[5] T. M. Tran et al., Digest of this conference

[6] J. Ph. Hogge et al., Digest of this conference

[7] B. Jödicke et al., Digest of this conference

[8] P.Muggli et al., Digest of this conference

[9] A. Pochelon et al., Contributed paper at the 16th SOFT Conference, (September 1990)

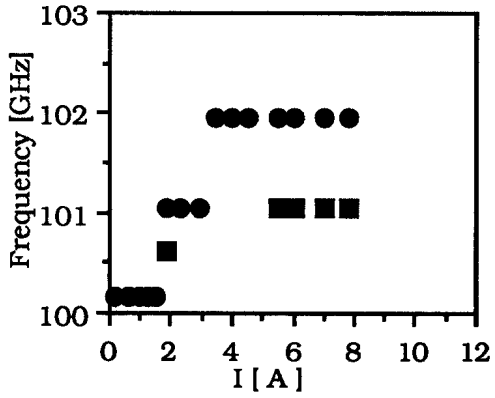

Figure 1. Measured frequency shift versus I (● : Main mode, ■ : Next mode)

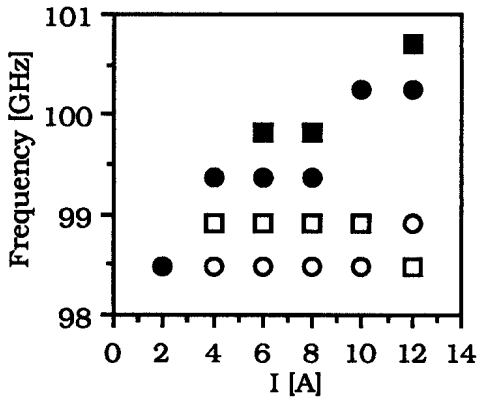

Figure 2. Computed frequency shift versus I (Open symbols: Without ΔV; ● : Main mode with ΔV,■ : Next mode with ΔV). B was not fitted to the case of Fig. 1.

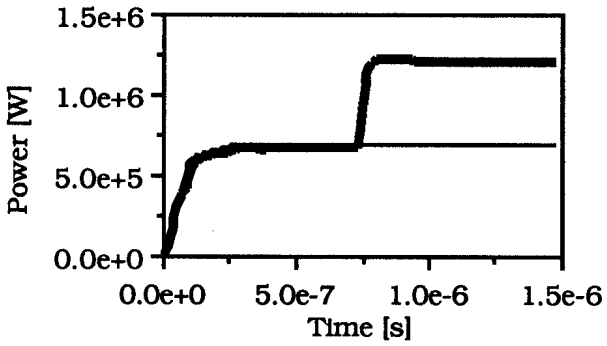

Figure 3.Variation of the power when V_b is increased from 70kV to 80kV (thick line). For comparaison, the thin line represents the power obtained when V_b is set at 80kV. I is equal to 50A , α to 1.5 and the transmission to 10%.

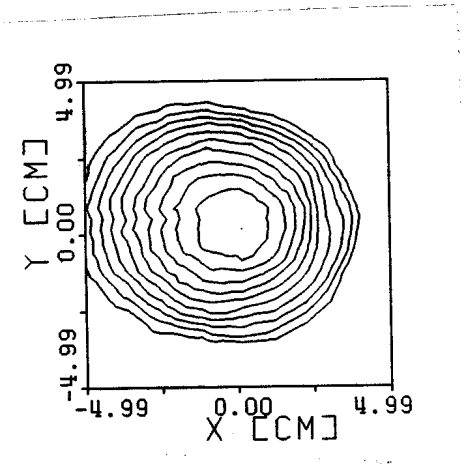

Figure 4. Pattern at the input of the HE_{11} waveguide, lines are separated by 3 dB.

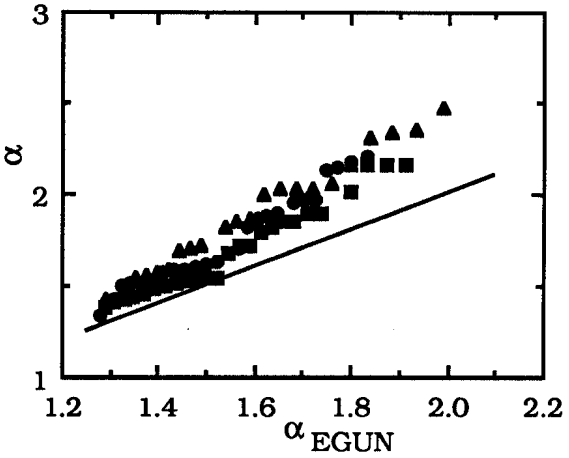

Figure 5. α deduced from the frequency of the BWO compared to α given by EGUN

Competition between the fundamental and the second harmonic in quasi-optical gyrotrons

T.M. Tran, F. Dufaux, S. Alberti, D. Monselesan, M. Pedrozzi and M.Q. Tran
Centre de Recherches en Physique des Plasmas
Association Euratom-Confédération Suisse
Ecole Polytechnique Fédérale de Lausanne
21, Av. des Bains, CH-1007 Lausanne

ABSTRACT

In quasi-optical gyrotrons (QOG) using Fabry-Pérot resonators designed to operate at the fundamental, the second harmonic interaction could be important due to the fact that the quality factor Q is an increasing function of the frequency. Emissions at frequencies twice the electron cyclotron frequency have been also observed experimentally in QOG as well as in cylindrical gyrotrons. In order to understand the nature of this unwanted emission and its effects on the efficiency of the quasi-optical gyrotrons, a simulation code, based on the slow time scale formalism is written to follow the time evolution of the fundamental as well as the higher harmonic modes. Results from the simulations of our 100 GHz QOG experiment will be presented.

1. SIMULATION MODEL

We assume that the spatial profile of the electromagnetic field is given by the cold cavity Gaussian TEM modes, as well as the wave frequencies. For the sake of simplicity, only the fundamental modes TEM_{00} in a confocal resonator are considered here (in the code, higher transverse modes and non-confocal resonators can be specified), in which case the frequencies satisfy the relation: $\omega_q = (q + 1/2)\Delta\omega$, $\Delta\omega$ being the frequency spacing of the cavity spectrum. The equations of motion of the particles in the simultaneous presence of the fundamental and the second harmonic fields can then be derived from the usual slow time scale assumption[1]. For an electron j, its perpendicular momentum $p_{\perp j}$, normalized to mc, its slow phase $\theta_j = \psi_j - \omega t_j$ where ψ_j is the rapidly varying electron phase and ω is a reference frequency close to the electron cyclotron frequency, and its transit time t_j evolve during one pass accross the interaction region, according to the following equations:

$$\frac{dp_{\perp j}}{dz} = -\frac{e}{mc^2} \sum_{n=1,2} \frac{n^n}{2^n n!} \frac{p_{\perp j}^{n-1}}{\gamma_j^{n-2}} \sum_l E_{l,n} f(z) G_{l,n}(y_{gj}) \times$$
$$\times \cos\left[n\theta_j + \left(\frac{n-1}{2} - l \right) \Delta\omega\, t_j - \phi_{l,n} \right] \qquad (1.a)$$

$$\frac{d\theta_j}{dz} = \frac{\Omega - \omega\gamma_j}{cp_z} + \frac{e}{mc^2} \sum_{n=1,2} \frac{n^n}{2^n n!} \frac{p_{\perp j}^{n-2}}{\gamma_j^{n-2}} \sum_l E_{l,n} f(z) G_{l,n}(y_{gj}) \times$$
$$\times \sin\left[n\theta_j + \left(\frac{n-1}{2} - l \right) \Delta\omega\, t_j - \phi_{l,n} \right] \qquad (1.b)$$

$$\frac{dt_j}{dz} = \frac{\gamma_j}{cp_{zj}}, \qquad p_{zj} = \text{const.}, \qquad \gamma_j = \sqrt{1 + p_{\perp j}^2 + p_{zj}^2}, \qquad (1.c)$$

where we have summed over the fundamental $n = 1$ and the harmonic $n = 2$ contributions as well as the longitudinal mode number l, $f(z) = \exp(-z^2/w_0^2)$ is the axial profile of the TEM_{00} Gaussian mode, $G_{l,n}(y_{gj}) = \cos[k_{l,n}y_{gj} - (l+n)\pi/2]$ is a geometrical coupling factor, $E_{l,n}$ and $\phi_{l,n}$ are respectively the amplitude and phase of the r.f. electric fields. These electric fields are assumed to be constant during one electron passage accross the interaction region, but from pass to pass, they can evolve slowly (low gain and high Q approximation) according to

$$\left[\frac{d}{dt} + \frac{\omega_n}{2Q_n}\right] E_{l,n}e^{i\phi_{l,n}} = \frac{4I}{\pi\epsilon_0 d w_0^2}\frac{n^n}{2^n n!}\int_{-\infty}^{+\infty} dz\, f(z)\frac{1}{N_p}\sum_{j=1}^{N_p}\frac{p_{\perp j}^n G_{l,n}(y_{gj})}{p_{zj}\gamma_j^{n-1}}\times$$
$$\times \exp\left[in\theta_j + i\left(\frac{n-1}{2} - l\right)\Delta\omega\, t_j\right] \qquad (2)$$

Note that the stored electromagnetic energy in the cavity induced by the n^{th} harmonic is simply given by

$$W_n = \frac{\pi\epsilon_0 d w_0^2}{8}\sum_l E_{l,n}^2. \qquad (3)$$

These equations are reduced to the ones obtained in Ref.[1] for a single harmonic n. Equilibrium model can also be deduced from these equations by taking $d/dt = 0$ in eq.(2). This has been done in Ref.[2] where only a single longitudinal mode was considered for each harmonic.

2. SIMULATION RESULTS

In the simulations presented below, the annular electron beam has a radius of $r_b = 2.13\,\text{mm}$, a velocity ratio $\alpha = 1.36$ and an energy of 66 KV. The resonator has a g factor of 0.326, a mirror separation $d = 33.7\,\text{cm}$ and transmission losses of 4.58% and 0.33% for the fundamental and the second harmonic respectively. The magnetic field is fixed at 3.96 T. All these values are consistent with the experimental set up described in Ref.[3]. The starting currents, computed from linear theory are 1.38 A and 0.52 A for the fundamental and the second harmonic respectively.

In order to describe well the phase space distribution function for the annular beam, 4096 simulation particles are loaded continuously at the entrance of the interaction region, using quiet start technique. Each harmonic field is described by 15 longitudinal modes distributed around the linearly most unstable frequency. A scan over the beam current has been made, with all the parameters specified above being held fixed, and the results at saturation are shown in Figs.(1). For comparison, we have also included in Fig.(1.a) the saturated efficiency obtained when the second harmonic field is switched off. As shown in Fig.(1.b), the second harmonic, which has a lower starting current than the fundamental, tends to suppress the fundamental emission at currents slightly above the starting current for the fundamental. This effect is illustrated more clearly in the time evolution of the stored energies plotted in Fig.(2.a). Notice that the time scale involved in this mode competition is very large, compared to the linear growth time for both harmonics. Between $I = 2\,\text{A}$ and $I = 4\,\text{A}$, both harmonics are present simultaneously; however, as can be seen in Fig.(1.a), the fundamental emission seems to be very weakly affected by the second

harmonic. With larger current, the strong fundamental emission prevents the second harmonic to reach a higher saturation level as shown in Fig.(2.b). Although a small fraction of the second harmonic is still present, the fundamental operation is completely unperturbed by this second harmonic field [see Fig.(1.a)].

3. DISCUSSION AND CONCLUSION

A time dependent multimode code in which the competition between the fundamental and the second harmonic is taken into account, is developped, using the slow time scale formalism. In the simulation model, the AC as well as the DC (beam depression) space charge fields have not been included. So far, the simulations show that the second harmonic affects very weakly the fundamental operation, except very near the starting current. The fundamental frequency field, when it becomes sufficiently strong, always prevents the second harmonic to start, while in the experiment described in Ref.[4], it has been observed that the second harmonic can be excited non-linearly by the fundamental, in contradiction with the simulation prediction. Another experimental observation is the decrease of the total efficiency whenever a second harmonic frequency is detected while the simulations show only marginal influences coming from the second harmonic emission. In conclusion, more theoretical investigations on the slow time scale formalism, together with more detailed measurements have to be done to explain the nature of the second harmonic emission observed in the QOG experiment described in Ref.[4].

ACKNOWLEDGEMENTS

This work was partially supported by the Swiss National Science Foundation, grant No 2000–005651

REFERENCES

1. A. Bondeson, W.M. Manheiner and E. Ott, "Multimode analysis of quasi-optical gyrotrons and gyroklystrons", in *Infrared and Millimeter Waves*, K.J. Button, ed., p.309, 1983
2. T.M. Tran, A. Bondeson, S. Alberti and M.Q. Tran, "Harmonic emission in quasi-optical gyrotrons", in *Proc. 14th Int. Conf. on Infrared and Millimeter Waves, Würzburg*, F.R.G. 1989, SPIE **1240**, p.235
3. S. Alberti, M.Q. Tran, J.P. Hogge, T.M. Tran, A. Bondeson, P. Muggli, A. Perrenoud, B. Jödicke and H.G. Mathews, "Experimental measurements on a 100GHz frequency tunable quasi-optical gyrotron", *Phys. Fluids* **B2**,p.1654 (1990)
4. S. Alberti, M. Pedrozzi, M.Q. Tran, J.P. Hogge, T.M. Tran, P. Muggli, B. Jödicke and H.G. Mathews, "Experimental measurements of competition between fundamental and second harmonic emission in a quasi-optical gyrotron", Lausanne Report LRP 402/90 (April, 1990), to be published in *Phys. Fluids* **B2**, November 1990

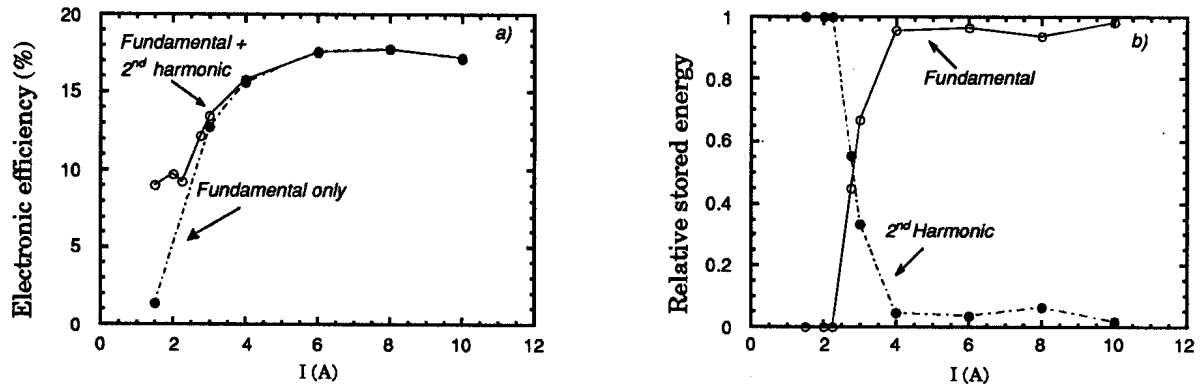

Fig. 1 The electronic efficiency *a)* and the relative stored energies at each harmonic *b)* at saturation, versus the beam current. The efficiency obtained when the second harmonic is switched off (dashed line) is added in *a)* for comparison.

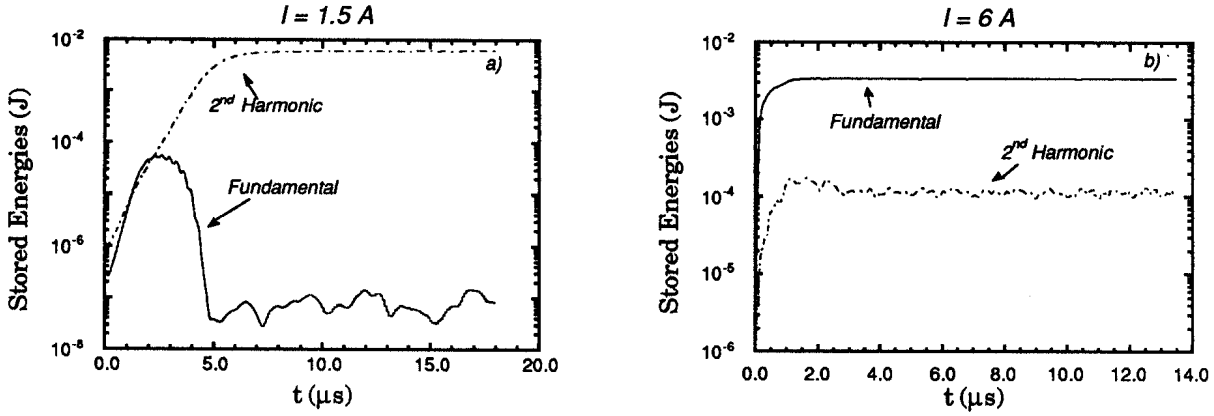

Fig. 2 Time evolution of the stored energy for each harmonic at $I = 1.5\,\mathrm{A}$ *a)* and $I = 6\,\mathrm{A}$ *b)*.

VELOCITY RATIO MEASUREMENT USING THE FREQUENCY OF BACKWARD WAVE OSCILLATIONS

P. Muggli, M.Q. Tran and T.M. Tran

Centre de Recherches en Physique des Plasmas
Association Euratom - Confédération Suisse
Ecole Polytechnique Fédérale de Lausanne
21, Av. des Bains, CH-1007 Lausanne, Switzerland

ABSTRACT

The operating diagram of a low-Q (Q_{diff}=160) TE^{o}_{01} gyrotron at 8GHz exhibits oscillations at frequencies in a range around both 7 and 10GHz. These frequencies are identified as the backward wave (BW) and forward wave (FW) components of the traveling TE^{o}_{21} mode. As the resonance condition of the BW depends on the average parallel velocity ($\langle v_{\|} \rangle$) of the beam electrons ($\omega_{BW} \cong \Omega_c/\gamma - k_{\|} \langle v_{\|} \rangle$), the measurement of ω_{BW}, for given Ω_c and γ, yields the value of the velocity ratio ($\alpha = \langle v_{\perp} \rangle / \langle v_{\|} \rangle$) and provides a diagnostic for α. Experimentally, we have measured ω_{BW} while varying I_{beam}, Ω_c and α. These results will be presented and compared to predictions of linear dispersion relation and of non-linear simulations.

2. INTRODUCTION

The experiment consists of an 8GHz low diffractive Q (Q_{diff} = 160), TE^{o}_{011} gyrotron. Gyrotron Backward Wave (Gyro BWO) oscillations in a range around 7GHz in the TE^{o}_{21} mode (Fig. 1) have been observed. In principle, the Gyro BWO instability is absolute since the negative group velocity of the backward traveling mode provides an internal feedback to the forward traveling cyclotron wave generated in the beam. However in practice, for a given interaction length (L_i), the beam current must exceed a threshold value before oscillations are observed. The oscillation frequency of the TE^{o}_{21} backward traveling mode (ω_{BW}) depends strongly on the average velocity ratio, defined as $\alpha = \langle v_\perp \rangle / \langle v_\parallel \rangle$, which is usually not measured. Thus the precise measurement of ω_{BW} could yield the value of α through the linear dispersion relation [1] or through non linear particle simulations [2].

3. GYRO BWO NUMERICAL ANALYSIS

The dependency of ω_{BW} on the physical parameters α, $U_{cathode}$, I_{beam}, B_0, r_{cavity}, and r_{beam} can be determined using the dispersion relation published by Chu [1]. A fully relativistic, self-consistent gyrotron simulation model [2] based on slow time-scale equations for the wave and for the particles' momenta and phase has been used to describe the Gyro BWO. The boundary conditions for the rf electric field (F) must be adapted to our gyrotron cavity. On the gun side, the backward wave impedance has to match the cavity impedance:

$$\frac{dF}{dz}\Big|_{z=0} = - ik_\parallel F.$$

The output power is reflected by the cut-off part of the cavity and travels without interaction to the load. On the collector side, the end of the BW interaction is defined by the fast change of $k_\parallel$, occurring in the output uptaper, which detunes the interaction ($\omega_{BW} \cong \Omega_c/\gamma - k_\parallel \langle v_\parallel \rangle$). We impose at $z=L_i$:

$$\frac{dF}{dz}\Big|_{z=L_i} = + ik_\parallel F.$$

The numerical simulations show that this condition is sufficient to insure that the electric field becomes very small for $z>L_1$. The straight part of the cavity is 20.5cm long and the interaction length is found to be around 24cm ($L_1 \cong 5.5$ - $6.0\ \lambda_{vacuum}$). Figure 2 shows an example of ω_{BW} versus α computed with these two methods.

4. EXPERIMENT

The gyrotron was designed to operate at 8GHz in the TE^{o}_{011} mode with a magnetic field in the range around 3.13kG. Its parameters are identical to the ones given in Ref. 2, except for the Q_{diff} which has been lowered to 160. The experimental mode map is shown on Fig. 3. For the measurement of α, the tube was operated as a Gyro BWO by applying a low magnetic field. It was necessary to match the output window to the TE^{o}_{21} mode by adding a second Al_2O_3 disk. This reduces the band structure otherwise observed on the frequency when varying the experimental parameters. The MIG gun has a diode structure and thus α is varied by changing the magnetic field in the cathode region.

5. RESULTS

For comparison, the value of α was computed with the EGUN [3] particle trajectory code (α_{EGUN}) using the experimental magnetic field profiles. Figures 4(a) and (b) show a plot of α inferred from ω_{BW} versus α_{EGUN}. The α inferred from ω_{BW} is calculated using both the linear dispersion relation and the non-linear particle simulation. The linear dispersion relation overestimates α_{EGUN} by more than 50% and gives unrealistic α values. Non linear calculations with realistic geometry and a cold beam are in good agreement with the predicted α values (α_{EGUN}) (+10% to +20%). Figure 5 shows that electron velocity dispersion in $v_\perp$ and $v_\parallel$ increases ω_{BW} and hence leads to an overestimation of α. Part of the discrepancy between the values of alpha inferred from ω_{BW} and the expected (α_{EGUN}) values can be attributed to velocity dispersion.

REFERENCES

[1] K.R. Chu, A.T Drobot, V.L. Granatstein and J.L. Seftor, "Characteristics and Optimum Operating Parameters of a Gyro Traveling Amplifier", IEEE Trans. Microwave Theory Tech., MTT-27, pp 178 - 187, 1979.

[2] P. Muggli, M.Q. Tran, T.M. Tran,, H.-G. Mathews, G. Agosti S. Alberti and A. Perrenoud, "Effect of Power Reflection on the Operation of a Low-Q 8GHz Gyrotron", IEEE Trans. Microwave Theory Tech., MTT-38, 1990.

[3] W.B. Hermannsfeldt SLAC - Report - 226, Standford Linear Accelerator Center, Standford, California, 1979.

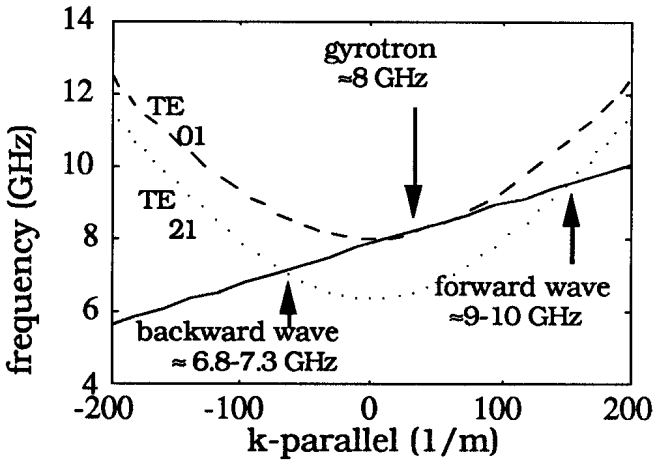

Fig. 1:

Dispersion curves for the TE^{o}_{01} and TE^{o}_{21} waveguide modes and the fast-beam cyclotron mode.

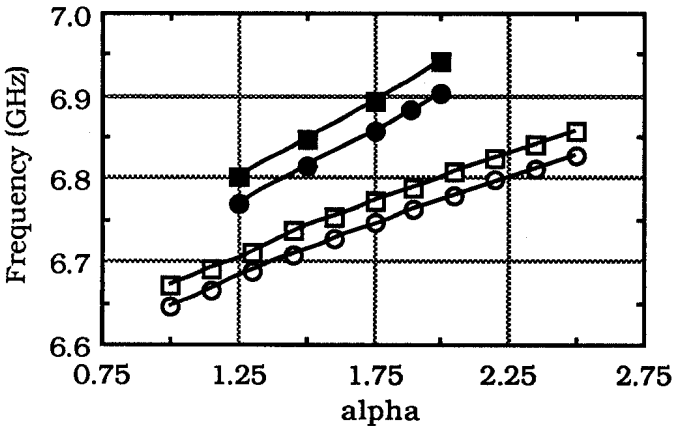

Fig. 2 : Dependency of the Gyro BWO frequency on α as computed with the linear dispersion relation (open symbols) and with the non-linear simulation for a cold beam (filled symbols) for $I_{beam}=4A$ (circles) and $I_{beam}=8A$ (squares).

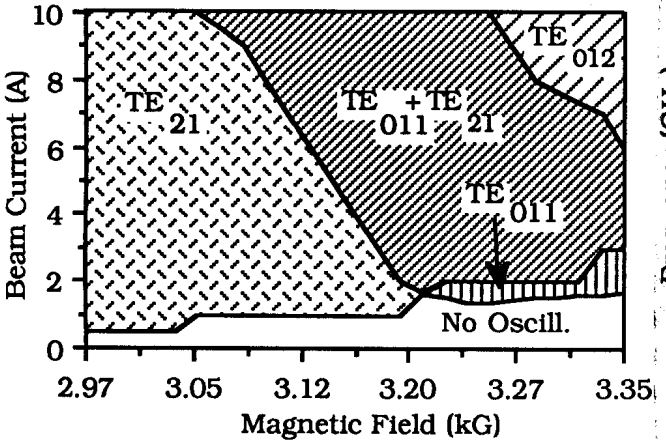

Fig. 3 : Experimental mode chart for α=1.7 and $U_{cathode}=75kV$

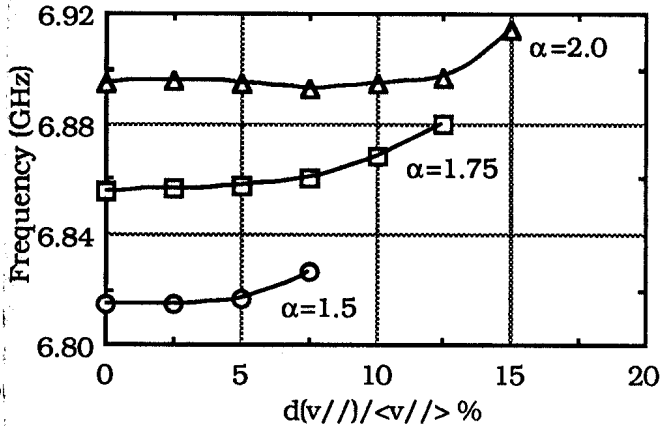

Fig. 5 : Effect of velocity dispersion on Gyro BWO frequency. For these calculations $\Delta\gamma=0$ is assumed and thus $\Delta v_\perp/\langle v_\perp\rangle=(1/\alpha^2)\Delta v_\parallel/\langle v_\parallel\rangle$.

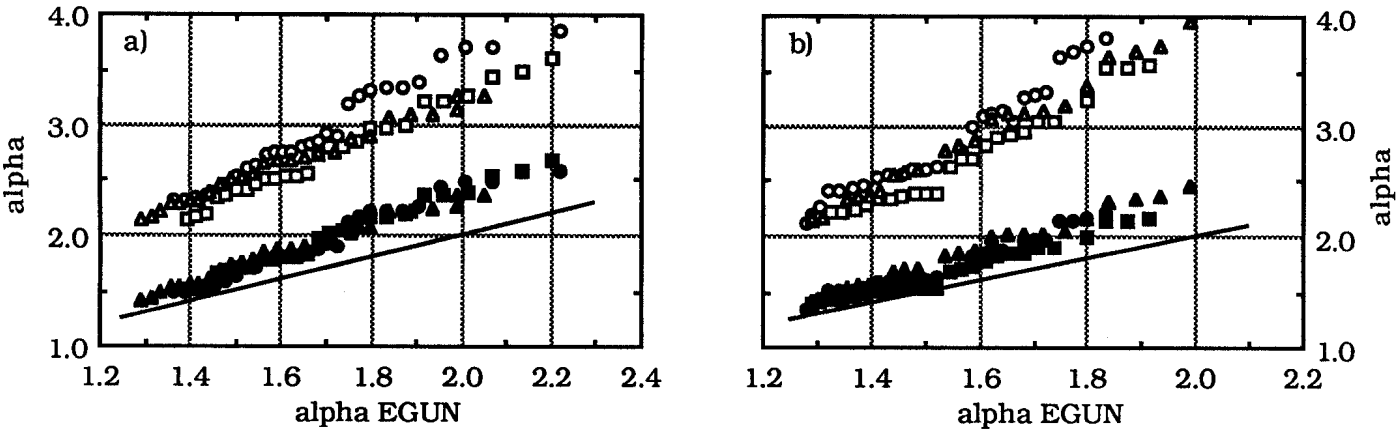

Fig. 4 : Comparison of α inferred from ω_{BW} to the α given by the EGUN code (using the experimental magnetic field profiles). The α inferred from ω_{BW} is calculated using the linear dispersion relation (open symbols) and the non-linear simulation (filled symbols). Data are plotted for: B_0= 2.970kG (circles), 3.033kG (squares), 3.095kG (triangles), $U_{cathode}=75kV$ and a) $I_{beam}=4A$, b) $I_{beam}=8A$.

OUTPUT COUPLING OF A QUASI-OPTICAL FABRY-PEROT RESONATOR BY MEAN OF A DIFFRACTIVE GRATING IN THE mm WAVE RANGE

J.P. Hogge, H.Cao, W.Kasparek*, T.M.Tran, M.Q.Tran

Centre de Recherches en Physique des Plasmas
Association Euratom-Confédération Suisse
Ecole Polytechnique Fédérale de Lausanne
21, Av. des Bains, CH-1007 Lausanne, Switzerland

*Institut für Plasmaforschung
Universität Stuttgart, Pfaffenwaldring 31, D-7000 Stuttgart 80, F.R.G.

ABSTRACT

In present quasi-optical (Q.O.) gyrotrons, the microwave power is coupled out by edge diffraction [1-3]. Results of cold tests and hot tests show that the output is non-Gaussian. Recently, we have tested successfully output couplers using a grating reflector which replaces one of the resonator mirrors. This type of coupling produces almost perfect Gaussian output patterns so that one can utilize an additional perfectly reflecting mirror to focus efficiently the output microwave beam into a corrugated HE_{11} waveguide.

1. DESIGN PRINCIPLES

Consider a resonator,one mirror of which is replaced by a grating arranged in -1 order Littrow mount [4], i.e. the -1 order is reflected back in the cavity and the 0^{th} order gives the output of the resonator. The efficiency in power for each order can be computed using an electromagnetic theory [4]. Figure 2 shows contours of constant efficiency for the -1 order of a grating with a sine profile in Littrow mount as a function of the angle of incidence θ and the groove depth h/d (where d is the groove period satisfying the Littrow condition), for the TM case. The shaded areas represent the -2 order efficiency for the second harmonic. It can be seen that, by a proper choose of θ and h/d, the resonator can be made frequency selective with respect to the second harmonic. This property is important since second harmonic emission was observed in gyrotrons [1]. As a preliminary experiment, we have cold tested such a resonator with a planar grating and straight uniformly spaced grooves. Results show that only one order of diffraction is observed, and that the measured efficiencies in the two orders agree with the calculations.

So far, only the case of a plane wave incident on a periodical planar grating has been discussed. If such a grating is used in the Q.O. gyrotron, the r.f. beam waist would be located on the grating mirror and the ohmic load would be too high. In order to alleviate this problem, the grooves should be designed such that the grating is matched to an incident Gaussian wavefront of given waist w_0 and curvature parameter g. A approximate design scheme can be found by noting that the -1 order Littrow mounting condition, which can be written as :

$$k\, d \sin\theta = \pi \qquad (1)$$

states that the phase of the incident wave changes by π between two successive grooves (separated by d). Knowing the phase profile of the Gaussian beam incident on the grating reflector (corresponding to the resonance profile of an equivalent resonator formed by two spherical mirrors), it is then possible to determine the shape of each groove, using the condition just stated above. For the 0^{th} order, the grating can be considered as a partially reflecting smooth surface. The use of a planar grating produces a diverging output beam and an elliptical mirror is necessary to refocus it into the HE_{11} waveguide, whereas a proper choice of the elliptical grating curvature produces a converging beam which is directly coupled. The coupling of a Gaussian beam to the HE_{11} mode of a corrugated waveguide has been shown to be optimal if the waist of the beam is placed at the entrance of the waveguide and if $w_0/a=0.594$ [6], where a is the radius of the waveguide.

2. EXPERIMENTS

a) Experimental set-up

The experimental set-up is shown in fig. 1 and is performed at frequencies around 100 GHz. The resonator is formed by a spherical metallic mirror and a diffracting grating placed in Littrow mount. The output pattern of the microwave beam is recorded by a diode mounted on an XY table, allowing scans over a 10x10 cm area. The receiving antenna is a rectangular horn; a simple rotation of 90° is then sufficient to measure the cross polarization content.
An estimate c^2 of the Gaussian power, of the diffracted beam is found by performing the following integration [5] :

$$c^2 = \frac{[\int_S dS\, E(x,y) \exp\{-\frac{(x^2+y^2)}{w_0^2}\}]^2}{[\int_S dS\, E^2(x,y)][\int_S dS \exp\{-\frac{2(x^2+y^2)}{w_0^2}\}]} \qquad (2)$$

where E(x,y) is the measured electric field and w_0 is an adjustable parameter. This formula gives an overestimated value since the phases are not taken into account. Nevertheless, as long as this integration is made near the waist (where the phase of a Gaussian beam is constant on a transverse plane) and the shape is close to a Gaussian, this estimation is quite good.

b) Planar grating with curvilinear grooves

A planar grating has been designed, following the description of the preceeding section . The advantage of this type of grating is that the exact shape of the grooves can be approximated by nearly concentric circles. The diffracted beam is divergent and an elliptical mirror is necessary to focalize it into the HE_{11} waveguide. The Figure 3a shows the pattern of a TEM_{00} mode measured at the mouth of the HE_{11} waveguide. No sidelobe is observed within 30 dB. The coupling factor c^2 is higher than 98%. Some transverse polarization is induced on the grating since the incident electric field is not purely TE, nor TM. The efficiencies being different, this induces a rotation of the polarization vector. In the present case, a fraction of 10% to 15% of the power is in the wrong polarization. Taking into account the depolarization losses, the coupling factor c^2 as well as the coupling factor of the ideal Gaussian beam to the HE_{11} mode [5], the overall efficiency is estimated to be 83%. This number can be somewhat increased by designing a cavity such that the grooves are less curved.

c) Elliptical grating with straight grooves

Using the design principles discussed above, we have found that if the grating is matched on an elliptical surface, the grooves are less curved and the spacing is rather uniform, thus the depolarization induced on the grating is minimized (the depolarization induced by the elliptical curvature of the grating should be small [7]). We have designed and manufactured an elliptical grating with constant spacing and straight grooves.The pattern at the entrance of the waveguide and at the output looks more distorted than in the other case, even though it is still close to a Gaussian beam.The measured cross-polarization loss is negligible (< 1%). The coupling factor c^2 is 93% and the overall efficiency is about 90%. The measured distorsion has been attributed to the fact that the Littrow condition is met on one point only for this particular grating. By manufacturing a grating with a non-constant period and possibly curvilinear grooves, the pattern might be improved.

3. CONCLUSION

It has been shown that the electromagnetic field of a resonant cavity can be coupled out very efficiently by a diffracting grating placed in Littrow mount. A comparison has been made between an planar grating with curvilinear grooves and an elliptical grating with straight grooves. The planar grating gives almost ideal Gaussian patterns but a non-negligible fraction of the output power is in the wrong polarization, whereas the elliptical grating does not, at the cost of some distorsion. For the time being , the efficiencies of both schemes are of the order of 85%. Improvements on both schemes are possible, leading to higher efficiencies. Applications to high power quasi-optical gyrotrons are envisaged.

REFERENCES

[1] S. Alberti, M.Q. Tran, J.P. Hogge, T.M. Tran, A. Bondeson, P. Muggli, A. Perrenoud, B. Jödicke and H.G. Mathews, Phys. Fluids **B2**, 1654 (1990).

[2] M. E. Read, M.Q. Tran, J.Mc Adoo and M. Barsanti, Int. J. Electronics **65**, 309 (1988).

[3] J. Ph. Hogge, A. Perrenoud, M.Q. Tran, S. Alberti, B. Isaak, P. Muggli, and T.M. Tran, Proc. 14th Int. Conf. on Infrared and Millimeter Waves, Würzburg, F.R.G., 1989, SPIE **1240** , 233 (1989).

[4] See for example: Electromagnetic Theory of Grating, R. Petit, Ed. (Springer Verlag, 1980).

[5] R.L. Abrams, IEEE Trans. Quant. El., **QE-8**,838, (1972).

[6] L.Rebuffi, J.P.Crenn, Int. J. IR&MM Waves,**10**,1279,(1989).

[7] J.A. Murphy,Int. J. IR&MM Waves, **8**,1165, (1987).

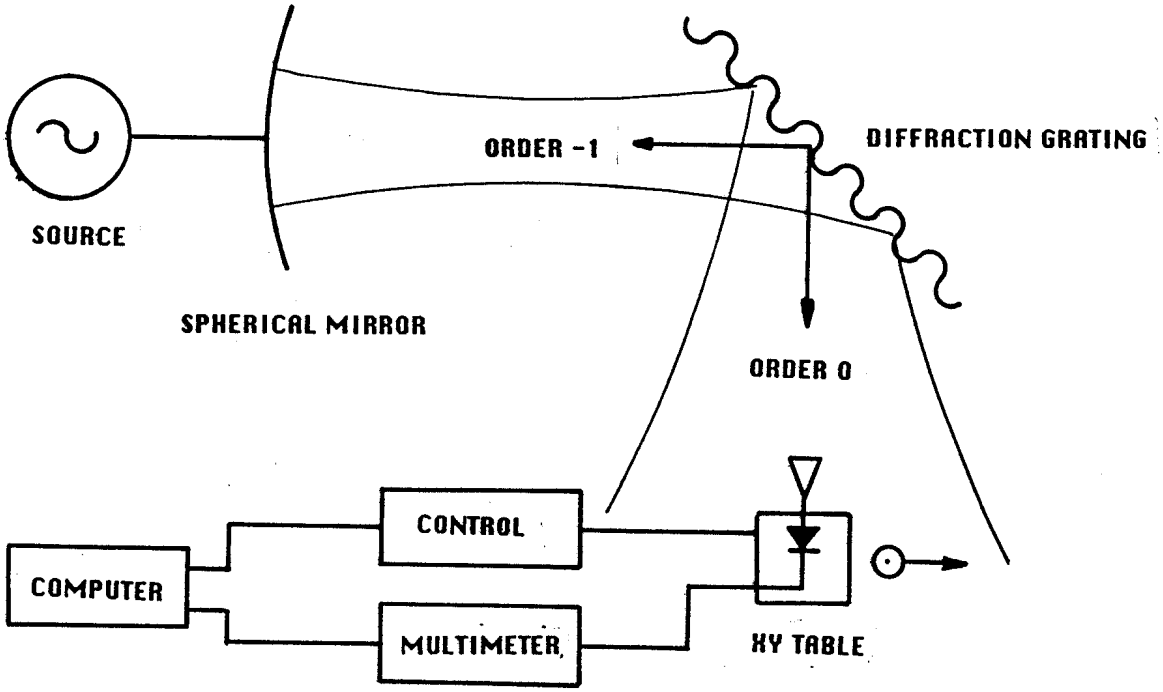

Figure 1

Experimental set-up

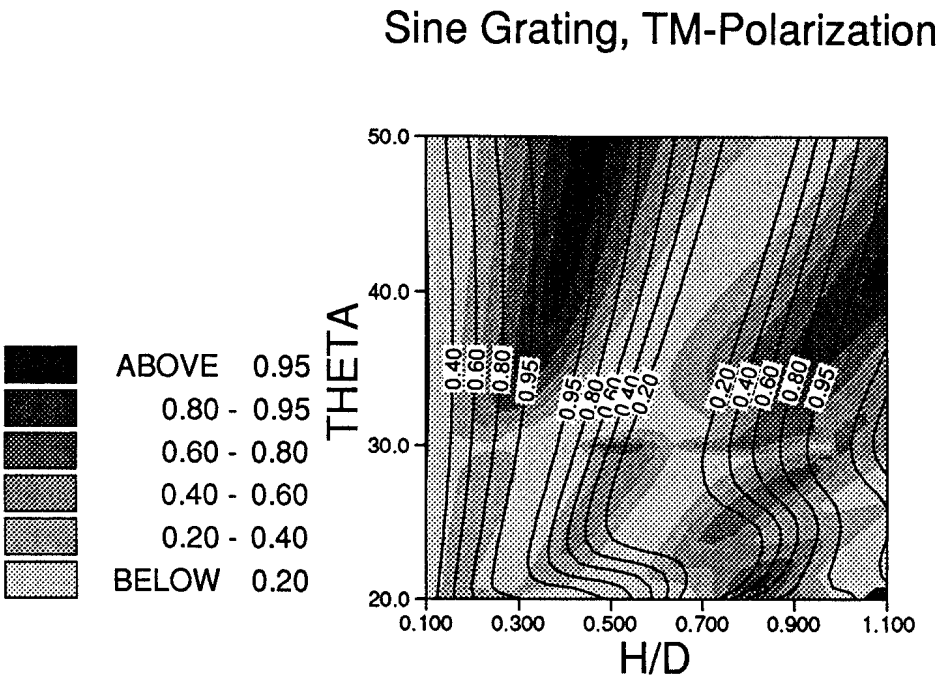

Figure 2

The -1 order efficiency for the fundamental (contour lines) and the -2 order efficiency for the second harmonic (shaded areas) versus the angle of incidence θ and the sinusoidal groove depth h/d, in the TM case, Littrow mount.

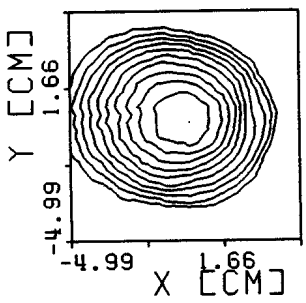

Fig. 3a Planar grating with curvilinear grooves: Pattern of a TEM_{00} mode measured at the entrance of the HE_{11} waveguide. Contours of equal intensity are separated by 3dB. The covered area is 10x10 cm. The g factor is -0.7.

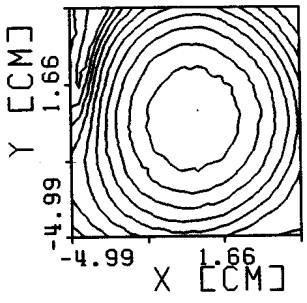

Fig. 3b Planar grating with curvilinear grooves: Pattern of the intensity of the field radiated by the HE_{11} waveguide, measured at 1 m of the output.

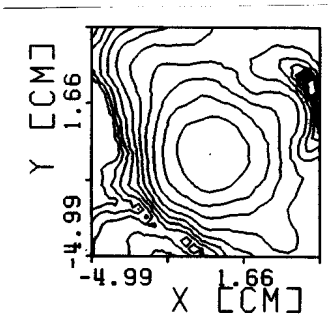

Fig. 4a Elliptical grating: Pattern of a TEM_{00} mode near the entrance of the waveguide. The g factor is +0.7. Contours are separated by 3 dB, area is 10x10 cm.

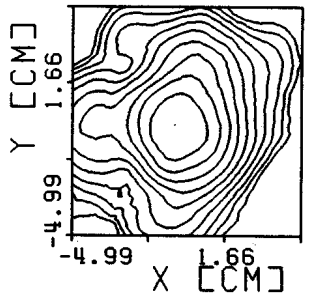

Fig. 4b Elliptical grating: Pattern of the intensity of the field radiated by the corrugated waveguide, measured at 35 cm of the output.